

A Cross-Match of 2MASS and SDSS. II. Peculiar L Dwarfs, Unresolved Binaries, and the Space Density of T Dwarf Secondaries

Kerstin Geißler, Stanimir Metchev

Department of Physics and Astronomy, State University of New York, Stony Brook, New York 11794-3800, USA

J. Davy Kirkpatrick, G. Bruce Berriman

Infrared Processing and Analysis Center, MC 100-22, California Institute of Technology, Pasadena, California 91225, USA

and

Dagny Looper

Institute for Astronomy, University of Hawaii, 2680 Woodlawn Drive, Honolulu, Hawaii'i 96822, USA

geissler@astro.sunysb.edu

ABSTRACT

We present the completion of a program to cross-correlate the SDSS Data Release 1 and 2MASS Point Source Catalog in search for extremely red L and T dwarfs. The program was initiated by Metchev and collaborators, who presented the findings on all newly identified T dwarfs in SDSS DR1, and estimated the space density of isolated T0–T8 dwarfs in the solar neighborhood. In the current work we present most of the L dwarf discoveries. Our red-sensitive ($z - J \geq 2.75$ mag) cross-match proves to be efficient in detecting peculiarly red L dwarfs, adding two new ones, including one of the reddest known L dwarfs. Our search also nets a new peculiarly blue L7 dwarf and, surprisingly, two M8 dwarfs. We further broaden our analysis to detect unresolved binary L or T dwarfs through spectral template fitting to all L and T dwarfs presented here and in the earlier work by Metchev and collaborators. We identify nine probable binaries, six of which are new and eight harbor likely T dwarf secondaries. We combine this result with current knowledge of the mass ratio distribution and frequency of substellar companions to estimate an overall space density of 0.005–0.05 pc⁻³ for individual T0–T8 dwarfs.

Subject headings: astronomical data bases: surveys—stars: low-mass, brown dwarfs — stars: peculiar — stars: individual (2MASS J00521232+0012172, SDSSp J010752.33+004156.1, 2MASS J01262109+1428057, 2MASS J07354882+2720167, 2MASS J09175418+6028065, SDSS J092615.38+584720.9, SDSS J121440.95+631643.4, 2MASS J13243559+6358284, 2MASS J14232186+6154005, SDSS J151603.03+025928.9, 2MASS J15423630–0045452, 2MASS J16154255+4953211, 2MASS J17310140+53104762, 2MASS J17373467+5953434)

1. INTRODUCTION

The cross-correlation of imaging surveys across a broad wavelength range allows efficient and reliable identification of photometrically unusual objects, such as cold brown dwarfs (e.g., Knapp et al. 2004; Chiu et al. 2006; Lodieu et al. 2007; Pinfield et al. 2008; Zhang et al. 2010), high-redshift quasars (e.g., Fan et al. 2001; Mortlock et al. 2009), or white dwarfs with unresolved (sub)stellar companions or debris disks (e.g., Rebassa-Mansergas et al. 2009; Steele et al. 2009). Searches for such objects are generally performed in a sequential manner, with candidates selected in one survey according to a set of desired color criteria and then confirmed in other surveys at similar locations but different wavelengths or epochs.

As we demonstrated in Metchev et al. (2008, henceforth, Paper I), this method is prone to overlooking an unknown fraction of objects of interest. The reason is that the initial step of the candidate selection process is performed on a single survey database, and as such it is limited by quality flag considerations that are inevitably used to constrain the number of potential candidates to include mostly astrophysically viable sources. While at high signal-to-noise levels ($\text{SNR} > 25$) quality flags are an efficient way to remove true contamination, at low signal-to-noise ratios “suspect” flag combinations (e.g., resulting from flux interpolation or from de-blending of closely-separated sources) carry a disproportionate weight in rejecting possible candidates. The effect of this process on the final object statistics can not be readily quantified. Consequently, the use of quality flags to screen against probable artifacts incurs an unknown level of incompleteness in any search for faint objects.

In Paper I we showed that the loss of viable candidates and the resulting incompleteness can be avoided if the initial round of candidate selection is done by using *cross-survey* colors, such as $z - J$ in the Sloan Digital Sky Survey (SDSS; Stoughton et al. 2002) and the Two-Micron All-Sky Survey (2MASS; Skrutskie et al. 2006). The extra verification obtained from joint z - and J -band identifications in SDSS and 2MASS allowed us to do away with all quality-flag constraints in either database. Undeniably, the approach is still prone to missing potentially interesting objects (e.g., very red z -band drop-outs). However, because

source detection in any imaging survey can be reliably and reproducibly defined solely in terms of signal-to-noise thresholds, the incompleteness incurred by requiring joint survey identification can be readily determined as a function of source flux. Hence, it is possible to obtain a statistically robust description of the resultant population of bona-fide objects down to very faint flux limits.

With many large-area imaging surveys completed over the past decade, multi-wavelength, multi-database cross-matching is at the heart of the planned functionality of electronic platforms that integrate astronomy data access, such as the Virtual Astronomical Observatory¹. However, while cross-correlations at scale are now feasible with modern computational facilities, the scientific validation of the results remains an open problem.

Along with the cross-survey candidate identification approach piloted in Paper I, we proposed a multi-step validation scheme for the extraction of bona-fide astrophysical objects. We based our investigation on a cross-correlation of the SDSS Data Release 1 (DR1; Abazajian et al. 2003) and the 2MASS Point Source Catalog (PSC; Cutri et al. 2003). The specific science goal was the discovery of all T dwarfs in the overlap of the SDSS DR1 and 2MASS footprints. For the purpose we selected all objects within $\Delta r = 6''.0$ of each other in the two databases that passed a $z - J \geq 2.75$ mag selection criterion, without imposing any quality flag constraints on candidate sources in either survey. (A complementary cross-survey identification approach, aimed at the detection of high-proper motion $\Delta r > 5''.0$ M, L, and T dwarfs between SDSS and 2MASS, was subsequently presented in Sheppard & Cushing 2008.) Our automated object validation approach, based on a comparison of the total number of positional identifications within the matching radius to the number of identifications that satisfied the color criterion, allowed us to throw out 99.9% of false candidates. Following an observational spectroscopic campaign, we accounted for all 13 known T dwarfs in SDSS DR1 and discovered two new ones (i.e., previous SDSS DR1 searches had unknowingly been 13% incomplete). With the candidate identification process well-defined—based solely on signal-to-noise ratios and colors—through Monte Carlo simulations we were able to accurately estimate the incompleteness of our search to T dwarfs of all flux levels. We consequently produced the first estimate of the space density of T dwarfs across all (T0–T8) spectral subtypes.

In the current paper we finalise the investigation commenced in Paper I, and characterize all other newly discovered objects, including L and M dwarfs. The $z - J \geq 2.75$ mag selection criterion was expected to produce objects as early as L3. Numerous candidate L dwarfs were indeed recovered, although their tally was subsequently restricted by an additional

¹<http://www.usvao.org/>

$i - z \geq 3.0$ mag color cut on all objects brighter than $i = 21.3$ mag. Altogether, 24 new and candidate L and T dwarfs were presented in Paper I, in addition to 19 that were already known in the SDSS DR1 footprint. Nineteen of the new candidates still required spectroscopic characterization, and 17 of these are presented here, while two could not be observed due to bad weather.

For details on the design and implementation of the SDSS DR1/2MASS cross-correlation, the criteria for excluding false candidates, and the final yield of the cross-match, we refer the reader to Paper I.

2. OBSERVATIONS

We observed 17 of the 22 candidate L dwarfs identified in Paper I. Spectra for an additional three were already published in Paper I. Two candidates remain unobserved to date: 2MASS J11571680–0333279 and 2MASS J21203387–0747208 due to clouds during the scheduled observing run.

We obtained low-resolution 0.9–2.5 μm spectra of the L dwarf candidates identified in the SDSS DR1/2MASS cross-match with the SpeX spectrograph (Rayner et al. 2003) on the NASA Infrared Telescope Facility (IRTF) between August 2007 and March 2008. The observations were taken in prism mode with the $0''.5 \times 15''.0$ or the $0''.8 \times 15''.0$ slit, resulting in resolutions of $R \sim 100 - 150$. The slit orientation was maintained to within 20° of the parallactic angle for all targets. We employed a standard A–B–B–A nodding sequence along the slit to record object and sky spectra. Individual exposure times were 180 s per pointing. Standard stars were used for flux calibration and telluric correction. Flat-field and argon lamps were observed immediately after each set of target and standard star observations for use in instrumental calibrations. Observation epochs and instrument settings for each science target are given in Table 2.

All reductions were carried out with the SpeXtool package version 3.2 (Cushing et al. 2004; Vacca et al. 2003), using an optimal spectroscopic extraction approach (Robertson 1986; Horne 1986). The reduced spectra were smoothed to the instrumental resolution corresponding to the chosen slit width, using the Savitzky-Golay smoothing kernel (Press et al. 1992).

The low resolution near-infrared (near-IR) spectra of the 17 new ultra-cool dwarfs are presented in order of increasing right ascension coordinate in Figure 1. SpeX spectra of M and L dwarf standards (Kirkpatrick et al. 1991, 1999) are overplotted for comparison.

3. SPECTRAL CLASSIFICATION AND UNRESOLVED BINARITY

3.1. Spectral Classification

The spectral classification of our targets was done primarily by comparison to near-IR SpeX spectra of optical M7–M9 (Kirkpatrick et al. 1991), optical L0–L8 (Kirkpatrick et al. 1999), and near-IR L9–T8 (Burgasser et al. 2006a) dwarf standards. We note that the L9 standard, 2MASSW J0310+1648, used by Burgasser et al. (2006a) to define a near-IR classification scheme for L8–T8 dwarfs, has an optical spectral type of L8 (Kirkpatrick et al. 2000).

Low-resolution SpeX spectra of most of the spectral standards were available from the SpeX Prism Spectral Libraries². Spectra of the L4 and L6 Kirkpatrick et al. standards were not available, and instead we used 2MASSI J1104+1959 and 2MASS J1010–0406, respectively. Both objects were originally classified in the optical and their near-IR colors are close to the average of the corresponding spectral types (Tab. 3). All standard M and L dwarf spectra cover a spectral range from 0.65 μm to 2.55 μm and have a resolution of $R \sim 120$, similar to that of our spectra. The full set of spectral standards is listed in Table 3.

We re-iterate that while the Kirkpatrick et al. (1991, 1999) M–L dwarf classification system is defined in the optical, we used near-IR spectra of the suggested standards for comparison to our data. The near-IR spectra of L dwarfs do not follow a monotonous sequence as a function of effective temperature as they do in the optical (McLean et al. 2003). The $>1 \mu\text{m}$ spectral shapes of L dwarfs reflect the varying depth of the photosphere as affected by the wavelength dependence of the combined dust and molecular opacity in the atmosphere (Ackerman & Marley 2001). For this reason we limited our spectroscopic classification to the 0.95–1.35 μm region, avoiding most of the strong H₂O absorption between 1.3–1.5 μm , and ensuring sampling of the temperature-sensitive short wavelength continuum. The classification itself was obtained by using χ^2 minimization to find the best-matching standard spectrum. For comparison, we also computed spectral types based on χ^2 minimization over most of the 0.95–2.35 μm region of our spectra, excluding only the low signal-to-noise regions (1.35–1.45 μm and 1.80–2.20 μm) in the midst of the near-IR H₂O bands. Spectral types for all of our objects are listed in Table 4 and alongside the plotted spectra in Figure 1.

²<http://web.mit.edu/ajb/www/browndwarfs/spexprism/>

3.2. Spectral Binary Fitting

To investigate if binarity may be the underlying reason for some of the peculiar features observed in the presented L dwarf sample, we fitted single and composite spectra to the data. For a comprehensive description of the fitting procedure we refer the reader to Cushing et al. (2008) and Burgasser et al. (2010).

A set of 190 single and composite 0.90–2.55 μm spectra was constructed using the chosen L0–L9 and T0–T8 spectral standards as templates. In order to flux-calibrate the spectra, all templates were scaled with respect to one another according to the K_s magnitude vs. spectral type relation defined by Looper et al. (2008a), before generating the composite spectra. The spectra of all composite templates were then allowed to freely scale to the spectra of the science targets. The best-fit composite spectrum for each candidate was determined by calculating a weighted χ^2 statistic, with the individual wavelength bins (detector pixels) weighted by their spectral bandwidth: $w_i = \Delta\lambda_i$ (see Burgasser et al. 2010; Cushing et al. 2008). The fit was performed only over the 0.95–1.35 μm , 1.45–1.8 μm , and 2.0–2.35 μm wavelength ranges in order to avoid regions of low signal and high telluric absorption.

As mentioned by Burgasser et al. (2010), the much larger number of composite (171) vs. single (19) templates implies almost certainly better χ^2 fits with composite rather than single object templates. We applied the one-sided F test to evaluate the significance of the best-fit composite spectrum using the η_{SB} statistic, defined by Burgasser et al. (2010, Eq. 2) as the ratio of the χ^2 values of the best-fit single template and the best-fit composite template. The number of degrees of freedom is $\nu = N_{\text{eff}} - 1$ to account for the scaling process during fitting, where N_{eff} is the effective number of data points in each spectrum. In a slight departure from the parameterization of Burgasser et al. (2010), we define N_{eff} as the number of *independent* resolution elements in our spectra, equal to the total number of pixels N divided by the number of pixels per slitwidth. Most of our spectra are taken with a 5 pix-wide ($0''.8$) slit, and a few with a 3 pix-wide ($0''.5$) slit (Table 2), and N_{eff} is either 59 or 99, correspondingly.

To rule out the null hypothesis, i.e., that a candidate is a single object, at the 99% confidence level (CL), we require $\eta_{SB} > 1.85$ for the 5 pix-slitwidth spectra or $\eta_{SB} > 1.61$ for the higher-resolution 3 pix-slitwidth spectra. In order to test the reliability of the best-match composite fit, we varied the initial flux-calibration of the templates within the RMS scatter of the K_s magnitude vs. spectral type relation (± 0.33 mag; Looper et al. 2008a). We repeated the χ^2 minimization 1000 times for each of the binary candidates, randomly varying the flux-calibration of the primary and the secondary independently within the range permitted by the scatter in the relation.

Considering that four of the nine L dwarf standards that are used as spectroscopic

templates are actually binary systems themselves (the L2, L3, L5, and L7 standards from Kirkpatrick et al. 1999), the individual spectral types of the components should not be taken as definitive. Nevertheless, a superior χ^2 fit of a composite template to any of the candidates suggests that the object is probably an unresolved binary system.

4. RESULTS

Fifteen of the new candidates are confirmed either as L dwarfs, or as unresolved binaries with L composite spectral types, and two as M dwarfs. Among the new L-type objects, three are identified as unresolved binaries (L+L or L+T), two are peculiarly red, and one is peculiarly blue. In our selection of objects with peculiar colors, we have followed the construct of Faherty et al. (2009), requiring that an object has a $J - K_s$ color that is either 2σ or 0.4 mag away from the mean for its spectral subtype.

An additional search for unresolved binarity among the L and T dwarfs reported in Paper I reveals that two of those L dwarfs and four of the T dwarfs are also likely binaries. One of the T dwarf binaries has been spatially resolved into two components by Burgasser et al. (2006a), two others have been suggested as probable binaries from spectral template fitting by Burgasser et al. (2010), and the remaining one is new.

We first discuss the probable binary systems, then the peculiarly blue or red L dwarfs, and eventually select ordinary L and M dwarfs discovered in the cross-match.

4.1. Candidate Binaries

Three of our 15 L dwarfs are significantly better fitted by a composite than by a single template at the >99% confidence level. Best-fit single and composite spectra for these binary candidates are shown in Fig. 2. Six additional unresolved binaries from the Paper I sample are presented in Fig. 3. Table 5 lists the two most likely spectral template combinations for each of the unresolved binary candidates, along with the fraction of Monte Carlo outcomes in which the given combinations were the best fit ones. The individual systems are discussed in the following.

4.1.1. *New Candidate Unresolved Binaries*

2MASS J0735+2720. The 0.95–1.35 μm continuum of this object is best-fit by an L1 standard (Fig. 1(a)). However, with a $z - J$ color of 3.03 ± 0.17 mag, 2MASS J0735+2720 is red compared to the average for the L1 spectral subtype (Table 3). The H band peak is flat for an L1 dwarf and the K band peak is shifted towards the blue. Spectral fitting suggests that the spectrum of 2MASS J0735+2720 is a composite of an L1 and an L4 dwarf.

2MASS J1423+6154. If single, this dwarf would be classified as an L4 (Fig. 1(c)). However, the 2MASS colors and the SED are slightly blue in $J - H$ and $J - K_s$. Spectral fitting shows that the spectrum of 2MASS J1423+6154 is best reproduced by an L2 + T5 composite spectrum, with an L2 + T4 composite almost as likely.

2MASS J1737+5953. If single, this dwarf would be classified as a blue L9 (Fig. 1(f)), since its $J - K_s$ color is more than 2σ (or 0.4 mag) bluer than the average of the L9 subtype. The spectrum shows a marked methane absorption feature at 1.6 μm and the K band peak is rounded, with its maximum shifted slightly towards the red. The best-fit L5 + T5 composite template reproduces all of these spectral features. We note that 2MASS J1737+5953 is the only binary candidate for which we cannot formally claim binarity at the 99% confidence level ($\eta_{SB} = 1.55$, while the 99% threshold is $\eta_{SB} > 1.61$ for its 3 pix-slitwidth spectrum). However, the 1.6 μm methane absorption leaves little ambiguity about the presence of an unresolved mid-T component.

4.1.2. *Additional Binary Candidates from Paper I*

The L and T dwarfs reported in Paper I were not checked for unresolved binarity. We do so here, and find six more probable binaries (Fig. 3).

2MASS J0052+0012 was reported as a moderately blue L2 dwarf in Paper I, and was designated as peculiar. In fact, the object is only moderately blue in $J - K_s$ and not a $> 2\sigma$ outlier. Hence, the peculiar designation is unwarranted under the presently adopted definition, even if the color may be suggestive of unusual properties. The best-fit composite spectra indeed indicate that it is likely a combination of an L4/L2 dwarf and a T3 dwarf.

SDSS J1731+5310 was an already known L6 dwarf in the SDSS DR1 footprint, first announced by Chiu et al. (2006). The near-IR spectrum of SDSS J1731+5310 is best fit by a combination of an L5 and an L8 template.

SDSSp J0926+5847 is a T4.5 dwarf originally announced by Geballe et al. (2002). Our binary template fitting indicates two components: a T3 or a T4 dwarf and a T6 dwarf. Burgasser et al. (2006b) report a marginal elongation in high angular resolution 1.1 μm and 1.7 μm imaging of this object with NICMOS on the *Hubble Space Telescope*, from which they infer that SDSSp J0926+5847p is a binary with near-equal flux T4: + T4: components. This result is consistent with our inference of a T3/T4 and a T6 component.

SDSS J1214+6316 is a T3.5 dwarf originally discovered by Chiu et al. (2006). It has not been identified as a potential binary before. Our fitting indicates that it is a probable composite of a T2 and a T6 component.

2MASS J1324+6358 is a peculiar T2 dwarf reported independently in Looper et al. (2007) and in Paper I. Burgasser et al. (2010) suggest it is a possible L8 + T3.5 binary. Our fitting indicates that the most likely component spectral types are L9 and T2. Given the ambiguity among the optical spectra of L8 and L9 dwarfs, the two sets of findings are mutually consistent.

SDSS J1516+0259 is a $T0 \pm 1.5$ dwarf discovered by Knapp et al. (2004). Burgasser et al. (2010) list SDSS J1516+0259 as a highly probable binary candidate, with spectral types of $L7.5 \pm 1.1$ and $T2.5 \pm 2.2$. Our spectral fitting, based on a more limited number of spectral templates with integer-valued subtypes, yields spectral types of L9 and T0 for the two components.

4.2. A Peculiarly Blue Single L dwarf: 2MASS J1542–0045

The 0.95–1.35 μm spectrum of 2MASS J1542–0045 is most adequately fit by a single L7 template (Fig. 1(d)). No pairwise combinations of L or T dwarfs produce a significantly better match to the overall near-IR SED. Yet, the SED is suppressed redwards of 1.4 μm , and is responsible for its very blue 2MASS colors compared to other L7 dwarfs. The *K* band flux peak appears rounded with the peak slightly shifted towards redder wavelengths. The 2.3 μm CO absorption is weaker than in the comparison standards, while the H₂O absorption

at $1.4 \mu\text{m}$ is enhanced. 2MASS J1542–0045 also shows a deeper $0.99 \mu\text{m}$ FeH absorption line than in the L7 standard (see Fig. 4).

A comparison to the known blue dwarf SDSS J112118.57+433246.5 (L7.5, Chiu et al. 2006) reveals that both dwarfs have a similar spectral shape (Fig. 4). 2MASS J1542–0045 is marginally bluer than SDSS J1121+4332 in $J - K_s$ color, but its $0.99 \mu\text{m}$ FeH absorption is shallower. Indeed, 2MASS J1542–0045 shows all signs generally associated with the near-IR spectra of blue L dwarfs: an enhanced $1.4 \mu\text{m}$ H₂O absorption, weak CO absorption and, of course, an unusually blue SED (Burgasser et al. 2008b). Optical spectroscopy of 2MASS J1542–0045 is required to confirm its L7 designation.

4.3. Peculiarly Red Single L Dwarfs

Two peculiarly red, likely single L dwarfs are presented here: 2MASS J09175418+6028065 (§4.3.1) and 2MASS J16154255+4953211 (§4.3.2). An additional pair of peculiarly red L dwarfs were identified within the larger sample of SDSS DR1 L dwarfs: 2MASS J01262109+1428057 and 2MASS J01075242+0041563. The former was already discussed as a red, moderately low gravity L2 dwarf in Paper I. The latter was first identified and classified in the near-IR as an L5.5 dwarf by Hawley et al. (2002, SDSSp J010752.33+004156.1) and in the optical as an L8 by Hawley et al. (2002). We note the very red $J - K_s$ color of this object, and also designate it as a peculiar L8.

4.3.1. 2MASS J0917+6028

This dwarf was already noted for its unusually red $z - J$ color in Paper I, although no spectrum was available at that time. At $z - J = 3.48 \pm 0.32$ mag, it: (1) has the reddest $z - J$ color of any of the L and T dwarfs found in the entire SDSS DR1/2MASS cross-match, (2) is one of the reddest known L dwarf, and (3) is as red as mid-T dwarfs (see Table 3).

The spectrum of 2MASS J0917+6028 (Fig. 1(a)) cannot be fit by any of the L or T spectral standards, although we note that the lack of methane absorption precludes it from being a T dwarf. A conspicuous emission feature near $2.17 \mu\text{m}$ is a likely result of the incomplete removal of broadened Brackett γ absorption in the telluric standard. *Spitzer Space Telescope* 3.6–8.0 μm photometry presented in Paper I places it among other mid-L dwarfs, although slightly redder in $[4.5\mu\text{m}] - [5.8\mu\text{m}]$ color (see Figure 4 in Paper I).

We tentatively classify 2MASS J0917+6028 as an L5 dwarf. The overall spectrum is much redder than that of any of the standards, even though curiously the 2MASS PSC colors

do not reflect it. Near-IR colors computed from the spectrum are in disagreement by up to 2σ with the 2MASS colors, and classify 2MASS J0917+6028 as red outlier with a $J - K_s$ color more than 0.4 mag redder than the average.

Considering its red SED shape, 2MASS J0917+6028 is likely dusty and could be young. Better agreement is achieved with the spectrum of G196–3B (Allers et al. 2007), a 60–300 Myr L2 dwarf. The shallow K I absorption at $1.17\ \mu\text{m}$ and $1.25\ \mu\text{m}$ suggests low surface gravity. Figure 5 compares 2MASS J0917+6028 to G196–3B and Fig. 6 compares it to the even younger (1–50 Myr) L0 dwarf 2MASS J0141–4633 (Kirkpatrick et al. 2006), both of which appear to have stronger K I absorption features.

Even so, 2MASS J0917+6028 lacks the peaked H -band spectrum characteristic of low-gravity L dwarfs. The low SNR of 5–15 between $0.95\text{--}1.3\ \mu\text{m}$ prevents a reliable assessment of the strength of the gravity sensitive features. Finally, we note the $\sim 2.17\ \mu\text{m}$ bump in our spectrum, suggesting that hydrogen absorption features may not have been adequately removed from the telluric standard during post-processing. This likely affects the H band continuum, and may have affected its spectral shape.

Besides low gravity, high metallicity may be a possible explanation for a redder SED.Looper et al. (2008b) noted that theoretical models with higher metallicity result in overall redder SED’s than solar metallicity models. Higher metallicity would not result in a peaked H -band spectrum. However, in the absence of low gravity we would expect stronger alkali line absorption, unlike what is observed.

4.3.2. 2MASS J1615+4953

This dwarf has already been discovered by Cruz et al. (2007), where it is classified as an L4 from an optical spectrum. Here we tentatively classify it as an L6 (Fig. 1(e)). However, its $0.95\text{--}1.35\ \mu\text{m}$ flux is suppressed compared to the standard, making an assessment of the spectral type difficult.

The SED of 2MASS J1615+4953 is red throughout the near-IR. The K band peak is slightly shifted to the red, and the H band peak has a slightly pointed triangular shape. Alkali absorption lines are subdued in the $1.1\text{--}1.3\ \mu\text{m}$ region. All of these characteristics suggest that 2MASS J1615+4953 may be moderately young. The optical spectrum of 2MASS J1615+4953 also displays low gravity signatures (Cruz et al. 2007).

A comparison to G196–3B (Allers et al. 2007), a known young L2 dwarf (Fig. 5), reveals the similar spectral shapes of the two objects. Figure 6 compares 2MASS J1615+4953 to the

young L0 dwarf 2MASS J0141–4633 and 2MASS J0917+6028. Both 2MASS J1615+4953 and 2MASS J0917+6028 exhibit similar SED’s, with 2MASS J1615+4953 emitting stronger at $>1.55 \mu\text{m}$.

4.4. Notes on Select Ordinary L dwarfs

2MASS J0229–0053 has been classified as an L2 dwarf (Fig. 1(a)). While its SDSS / 2MASS $i - z$ and $z - J$ colors are very red, the spectrum is fully consistent with an L2 standard. The apparently peaked H band continuum may be an artifact of the low signal to noise of the observation (SNR ~ 12). The alkali line absorption strengths are comparable to a standard L2 dwarf, and the overall SED differs significantly from that of the lower-gravity L2 dwarf G196–3B (Fig. 5).

2MASS J1308+6103 has been classified as an L2 (Fig. 1(c)). The dwarf has a slightly red $z - J$ color ($\simeq 1 \sigma$ above the average) for its spectral type, but the $0.95\text{--}1.35 \mu\text{m}$ continuum is consistent with L2.

2MASS 1414+0107 has been classified as an L4 (Fig. 1(c)). The spectrum displays deeper water absorption between $1.35 \mu\text{m}$ and $1.5 \mu\text{m}$, and again at $1.9 \mu\text{m}$ than the comparison spectra.

2MASS J1534+0426 has been given only a tentative classification, L0: (Fig. 1(d)), because the spectrum has a low signal-to-noise ratio (SNR ~ 10).

2MASS J1716+2945 has been classified as an L3 (Fig. 1(e)). The blue 2MASS $J - K_s$ color ($\gtrsim 1.5 \sigma$ below the average) is inconsistent with the spectrum, which is well fit by the standard.

2MASS J2116–0729 has been classified as an L6 (Fig. 1(f)). However, the flux of 2MASS J2116–0729 is enhanced longward of $1.3 \mu\text{m}$, resulting in a slightly redder $J - K_s$ ($\sim 1.5 \sigma$) color than for the average L6 dwarf. The dwarf shows no signs generally associated with low gravity, leaving higher metallicity and/or enhanced atmospheric dust content as a possible explanation for the resulting red SED.

4.5. M dwarfs

Two of the candidate L dwarfs, 2MASS J0926+5230 (Fig. 1(b)) and 2MASS J1551+0151 (Fig. 1(e)) turn out to be late-M dwarfs. Their spectra are well fit by an M8 standard and show no unusual signatures of redness in the near-IR. This is despite the fact that the recorded SDSS/2MASS $z - J$ colors (2.77 ± 0.18 mag and 2.88 ± 0.28 mag, respectively) of the M dwarfs are much redder than the average for the M8 spectral type (2.07 ± 0.18 mag).

Given the applied color cuts the detection of M and early L dwarfs (L0–L2) is unexpected, but most likely explained by statistical fluctuations in the SDSS z and 2MASS J band photometry. With z and J magnitudes fainter than 19.4 mag and 16.5 mag, respectively, all of the ordinary early L dwarfs and the two M8 dwarfs are low SNR detections in both SDSS and 2MASS. Their magnitudes are uncertain (errors >0.10 mag), and so the $z - J$ colors have larger than typical errorbars ($\gtrsim 0.15$ mag). Given the likely thousands of late-M and early-L dwarfs in SDSS DR1, it is conceivable that a few of them would have $\sim 4\sigma$ discrepant $z - J$ colors simply due to statistical variance in the number of recorded photons. A simple comparison of the reported 2MASS colors of our targets with ones synthetically generated from the SpeX spectra confirms this notion: the low-SNR 2MASS photometry is rather broadly scattered around the one-to-one correspondence line with the much higher SNR synthetic colors (Fig. 7).

5. Discussion

5.1. The Fraction of Binary or Peculiar L and T Dwarfs

The SDSS DR1 and 2MASS PSC cross-match returned a total of 26 L dwarfs: 8 previously known, 3 presented in Paper I, and 15 presented here (see Paper I for a complete list). For 22 of the 26 L dwarfs near-IR spectra are available either from the present data, or from Paper I, or from the SpeX Prism Spectral Libraries. Six of these 22 L dwarfs have discrepant $J - K_s$ colors (based on synthetic photometry over the SpeX spectra), which is $>2\sigma$ or 0.4 mag away from the mean for their spectral subtype. This number includes one blue L dwarf, four red L dwarfs and one candidate unresolved binary (a blue color outlier; Table 4). The remaining four unresolved L dwarf binary candidates have $J - K_s$ colors within the 2σ range for their respective composite spectral types. We also checked the 15 known T dwarfs in SDSS DR1 for binarity, and found four probable binaries, one of which is a red color outlier (Table 4). After removing candidate unresolved binaries, none of the remaining T dwarfs have peculiar $J - K_s$ colors or SEDs.

Among the 278 L dwarfs in the proper motion study of Faherty et al. (2009), 11 (4.0%) and 22 (7.9%) were classified as blue and red outliers, respectively, based on their $J - K_s$ colors. All of these objects were considered regardless of binarity, i.e., their spectral types are potentially composite. In our sample of 22 L-composite dwarfs for which we have available spectra, we would thus expect one blue and two red dwarfs. The factor of two higher rate of discovery of red L-composite dwarfs is not unusual given the color bias of our SDSS/2MASS cross-correlation, and attests to the efficiency of the $z - J$ color selection in identifying peculiarly red objects. The factor of two higher fraction of blue color outliers (in $J - K_s$) is intriguing, although only marginally discrepant with expectations. It is possible that the $z - J \geq 2.75$ mag criterion enhances sensitivity to mid-L plus mid-T dwarf binaries, whose $z - J$ colors are artificially reddened by the T component’s J -band flux. The J -band flux peak of the T dwarf in these systems would also make the composite $J - K_s$ color peculiarly blue, such as in the L5+T5 candidate binary 2MASS J1737+5934 (§ 4.1.1).

The number of L and T dwarf binary candidates identified in our analysis approximately agrees with statistical expectations from published results. Goldman et al. (2008) compile data on high angular resolution imaging observations of L and T dwarfs and find that 24 out of 130 ($18.5\%_{-2.9}^{+3.8}$) L0–L9.5 dwarfs and 8 out of 38 ($21\%_{-5}^{+8}$) T0–T8 dwarfs are resolved binaries (see also Burgasser 2007). The corresponding expectations are for four L-composite type and three T-composite type binaries in our sample. The observed numbers are five and four, respectively, again marginally higher than the expectations. Our inferred frequencies of L and T dwarf binaries in our flux-limited samples of 22 L and 15 T dwarfs, for which near-IR spectra were available, are $23_{-7}^{+11}\%$ and $27_{-8}^{+13}\%$, respectively, conditional on the confirmation of all candidate unresolved binaries.

5.2. The Space Density of Isolated T Dwarfs and T Dwarf Secondaries

One of the main results of Paper I was a determination of the space density of T dwarfs in the solar neighborhood. In that paper we announced the discovery of two T dwarfs in addition to the 13 already known in the SDSS DR1 catalog. Based on a Monte Carlo analysis of the SDSS and 2MASS detection limits, we estimated a space density of $0.007 \pm 0.003 \text{ pc}^{-3}$ (95% confidence interval) for T0–T8 dwarfs within ≈ 90 pc of the Sun.

We do not report any new T dwarfs here, but we do report altogether nine candidate unresolved binaries, in eight of which one or both of the components are T dwarfs (§4.1). It is pertinent to discuss whether the T dwarf space density estimate of Paper I needs revision.

As far as composite spectral types of unresolved T dwarf systems are concerned, a

revision is not warranted. In Paper I we simulated the space density of unresolved T dwarf systems, regardless of whether they were individual objects or close binaries with a T-composite spectral type. Since none of the newly reported objects have T-composite spectral types, the space density on T dwarf systems remains the same.

Given our analysis of unresolved binarity, we are now in a position to determine the space density of T dwarfs regardless of their multiplicity, i.e., to estimate the number of individual T dwarfs among both isolated objects and multiples. We note that our SDSS/2MASS cross-match was not ideally designed to answer this question, since unresolved T dwarf companions to much earlier-type stars would not be recovered. Any binary system containing a T secondary and a primary earlier than L3 will have a composite spectral type $<L3$, and hence will most likely be excluded by the $z - J \geq 2.75$ mag criterion. E.g., a close binary like SCR 1845–6357A/B (M8.5/T6; Biller et al. 2006) would not have been picked up. Nevertheless, the frequency of unresolved T dwarf companions can be estimated from the current knowledge of binary and individual (sub)stellar populations, and constrained from the present analysis.

In Paper I unresolved T dwarf binarity was simulated by simply doubling the flux of an individual dwarf at any given T subtype, i.e., by assuming a mass ratio distribution that is a delta function at $q \equiv M_2/M_1 = 1$. This is an adequate approximation for very low mass binaries, whose mass ratio distribution is sharply peaked near unity (Burgasser 2007). A more comprehensive estimate of the frequency of T dwarf companions requires assumptions of the stellar mass function, the frequency and mass distribution of low-mass substellar companions to more massive brown dwarfs and stars, and the star formation history of the Milky Way galaxy. We attempt only an approximate estimate here.

Using a Kroupa (2002) multi-part power-law mass function for single stars, binarity rates of objects with B to T spectral types from the literature ($\sim 80\%$ for AB stars, Shatsky & Tokovinin 2002; Kouwenhoven et al. 2005; $\sim 55\%$ for FGK stars, Duquennoy & Mayor 1991; 25%–42% for M stars, Leinert et al. 1997; Fischer & Marcy 1992; $\sim 20\%$ for late-M to T dwarfs, (Burgasser 2007, and references therein), and a mass ratio distribution for both stellar and substellar companions of the form $\Gamma(q) = dN/dq \propto q^\beta$ ($\beta \approx -0.4$ for B–K stars, Shatsky & Tokovinin 2002; Kouwenhoven et al. 2007; Metchev & Hillenbrand 2009; $\beta \approx 0.3$ for M0–M6 stars, based on results from the 9 pc M dwarf multiplicity survey of Delfosse et al. 2004; and $\beta \sim 5$ for late-M, L, and T dwarfs, Burgasser 2007), we find that $\sim 13\%$ of all companions in binary systems are substellar ($M_2 < 0.072M_\odot$) and that their space density is $\sim 0.024 \text{ pc}^{-3}$. Adopting a uniform age distribution over 0–10 Gyr and assuming that any object with an effective temperature between 500 K and 1400 K is a T dwarf, an application of the substellar evolutionary models of Baraffe et al. (2003) indicates that $\approx 85\%$ of all

$>0.01 M_{\odot}$ brown dwarf companions are T dwarfs. Hence the estimated space density of T dwarf *secondaries* based on the above assumptions is $\rho_{\text{T comp}} \sim 0.02 \text{ pc}^{-3}$.

Not all of the above parameters are well constrained, and our estimate can vary substantially in either direction given the parameter uncertainties. The greatest weight is carried by the adopted parameters for the population of very low mass (VLM) primaries. Seventy percent of all T dwarf companions are estimated to orbit a $<0.1 M_{\odot}$ primary, and varying either the VLM star IMF power law index ($\alpha_0 = 0.3 \pm 0.7$; Kroupa 2002) or multiplicity fraction ($20 \pm 10\%$; Burgasser 2007) within their empirical uncertainty ranges can affect the estimate for $\rho_{\text{T comp}}$ in either direction by up to 50% or 35%, respectively. The empirical evidence for the space density of isolated T dwarfs indeed indicates that α_0 is at most 0 (Paper I; Reylé et al. 2010) or perhaps -0.5 (Pinfield et al. 2008; Burningham et al. 2010). These result in $\rho_{\text{T comp}} = 0.017 \text{ pc}^{-3}$ or 0.014 pc^{-3} , respectively.

Variations in the power law index β_{VLM} of the mass ratio distribution $\Gamma(q)$ of VLM stars have much less of an impact ($<5\%$), since the distribution is so strongly peaked near unity. We note, however, that the difference between $\beta_{\text{VLM}} \sim 5$ and the power law index $\beta_{\text{M}} = 0.3$ of the mass ratio distribution of $>0.1 M_{\odot}$ field M dwarfs is large compared to that between β_{M} and the power law index β_{BK} for higher mass, B–K type binaries. The $\beta_{\text{M}} = 0.3$ value was obtained as our own fit ($\chi^2 = 1.2$) to the Delfosse et al. (2004) mass ratio distribution of the 9 pc M-dwarf binary sample, and has a 68% confidence interval of $[-0.4, 3.2]$. Delfosse et al. (2004) find that their combined radial velocity and high angular resolution survey is nearly 100% complete to stellar companions with periods up to 10^5 years and 75% complete to brown dwarf companions with periods up to 10^3 years, so no significant incompleteness corrections are needed. Allowing β_{M} to increase up to the upper limit of its 68% confidence interval decreases the space density of T dwarfs by 25%, all else being fixed. Changes in the power law index β_{BK} of the mass ratio distribution of higher-mass binaries have a $<5\%$ impact on the space density of T dwarf companions, since B–K stars are estimated to harbor only $\sim 2\%$ of all T dwarf companions in the present framework of assumptions.

Finally, systematic uncertainties in the substellar evolutionary models impact our temperature-based definition of a T dwarf: a $500 \text{ K} < T_{\text{eff}} < 1400 \text{ K}$ object. A 30% decrease in the equivalent mass predictions for this temperature range for all 0–10 Gyr-aged substellar objects decreases $\rho_{\text{T comp}}$ by 35%. A similar increase in the predicted masses increases $\rho_{\text{T comp}}$ by 10%.

Overall, our analytical estimate the space density of T dwarf companions lies in the $0.005\text{--}0.04 \text{ pc}^{-3}$ range. Values near 0.02 pc^{-3} are favored for the nominal values of the adopted Kroupa (2002) IMF, binary fraction, and mass ratio distribution parameters. Values

near 0.015 pc^{-3} are obtained for flat or slightly increasing forms of the substellar portion of the mass function, as motivated by the population of T dwarfs in the solar neighborhood.

The above estimate is marginally higher than the $0.004\text{--}0.01 \text{ pc}^{-3}$ space density (95% confidence interval) of unresolved T0–T8 dwarf systems from Paper I. Our analysis does double-count certain types of widely-separated T dwarf companions. If sufficiently bright, these could be identifiable as isolated objects (e.g., Gl 337C/D, Gl 570D, etc) in seeing-limited surveys such as SDSS or 2MASS, and would contribute towards the isolated T dwarf space density. At the same time, we count these secondaries as part of the companions that are generally undetected or unresolved by SDSS or 2MASS. However, the effect of the double counting turns out to be negligible. The majority of known widely-separated T dwarf companions detected by seeing-limited imaging are associated with primaries with A–K spectral types, i.e, more massive than $0.5 M_{\odot}$. As we already discussed, we estimate that less than 2% of all T dwarf companions orbit $>0.5 M_{\odot}$ stars. We therefore conclude that T dwarfs exist at least as frequently, and perhaps even twice as frequently in binary systems with a higher-mass companion than as isolated objects.

Our now completed analysis of the SDSS DR1 and 2MASS PSC cross-match can also place an independent empirical lower limit on the frequency of unresolved T dwarf secondaries relative to isolated and composite T dwarf systems. This can be obtained from the ratio of the number of L+T or T+T probable binaries (eight, if all are confirmed) found in the cross-match to the total number of T dwarfs in the SDSS DR1 footprint (15; Paper I). We note that unresolved equal flux binary systems are over-represented by a factor of $2^{3/2} = 2.8$ (less if non-equal flux) in a flux-limited survey. Given eight candidate and confirmed unresolved binaries with T dwarf secondaries in our flux-limited sample, the actual relative frequency of unresolved T dwarf secondaries to T-composite systems in a volume-limited sample would be $\sim \frac{8}{2.8} : 15 \approx 20\%$. This is a lower limit, since it only includes T companions to \approx L3 dwarfs or later. Additional unresolved T companions might also exist to the four L dwarfs (out of 26 total recovered in our cross-match), for which we do not have SpeX spectra to determine unresolved binarity (Section 5.1). Statistically, one of these would be expected to be an unresolved binary, with approximately equal probabilities of the secondary being an L or a T dwarf.

In summary, the frequency of T dwarf companions is at the least greater than $\approx 20\%$, and probably a factor of two higher than that of isolated T0–T8 dwarfs. Our broadest estimate for the space density of T type companions is thus between 0.001 pc^{-3} and 0.04 pc^{-3} , with the overall space density of T0–T8 objects, whether in binaries or in isolation, between 0.005 pc^{-3} and 0.05 pc^{-3} .

6. Summary

With this paper we have concluded a pilot undertaking, first described in Metchev et al. (2008), to cross-correlate the SDSS DR1 and 2MASS PSC databases over their 2099 deg² common area in search for rare objects: very red L and T dwarfs. The principal scientific results from the completed project are:

- the discovery of two additional T dwarfs in an already thoroughly perused region of the sky, both in SDSS and in 2MASS (Metchev et al. 2008);
- thus, a completion of the T dwarf sample in the SDSS DR1 footprint to within the combined SDSS/2MASS flux limits, and the first estimate of the space density of isolated T dwarfs (spectral types T0–T8; Metchev et al. 2008);
- thus, an empirical constraint on the field substellar mass function (Metchev et al. 2008), enabling predictions for the yield of future sensitive wide-area IR surveys;
- the identification of eight probable T dwarf companions in spatially unresolved L+T or T+T binary systems, five of which are new (this paper);
- hence, the first estimate of the space density of T dwarf secondaries, and a combined estimate of the space density of isolated and secondary companion T dwarfs (this paper);
- the discovery of an L dwarf (2MASS J0917+6028) with one of the reddest known optical minus near-IR ($z - J$) colors: a potential new laboratory for studying low-gravity or dusty substellar atmospheres, such as those of young extrasolar giant planets (this paper).

The above results were obtained by cross-correlating only the 2099 deg² overlap of the SDSS DR1 and 2MASS footprints. With SDSS-II recently complete and SDSS-III well under way, the 5.6 times larger area (11,663 deg²) of SDSS Data Release 7 (Abazajian et al. 2009) offers proportionately richer prospects. Combined with the opportunities presented by the on-going UKIRT Infrared Deep Sky Survey (UKIDSS; Lawrence et al. 2007) and *Wide-Field Infrared Survey Explorer* (*WISE*; Duval et al. 2004), the potential of cross-survey science has grown tremendously.

The completed project represents a successful demonstration of the feasibility and scientific merits of database cross-correlation and validation at scale. It has produced several valuable lessons on the computational logistics of cross-correlations, on the required understanding of the physical and statistical properties both of the target sources and of possible

contaminants, and on the need for judicious use of database quality flags for object discrimination. We anticipate that these lessons will be beneficial to larger, multi-wavelength cross-survey comparisons in the future.

This research has benefitted from the M, L, and T dwarf compendium housed at DwarfArchives.org and maintained by Chris Gelino, Davy Kirkpatrick, and Adam Burgasser. This research has benefitted from the SpeX Prism Spectral Libraries, maintained by Adam Burgasser at <http://www.browndwarfs.org/spexprism>. This research has benefitted from the Ultracool Dwarf Catalog housed at http://www.iac.es/galeria/ege/catalogo_espectral/index.html. This research has made use of data obtained from or software provided by the US National Virtual Observatory, which is sponsored by the National Science Foundation.

Facilities: IRTF (SpeX).

REFERENCES

- Abazajian, K., et al. 2003, *AJ*, 126, 2081
- Abazajian, K. N., et al. 2009, *ApJS*, 182, 543
- Ackerman, A. S., & Marley, M. S. 2001, *ApJ*, 556, 872
- Allers, K. N., et al. 2007, *ApJ*, 657, 511
- Baraffe, I., Chabrier, G., Barman, T. S., Allard, F., & Hauschildt, P. H. 2003, *A&A*, 402, 701
- Biller, B. A., Kasper, M., Close, L. M., Brandner, W., & Kellner, S. 2006, *ApJL*, 641, L141
- Bouy, H., Brandner, W., Martín, E. L., Delfosse, X., Allard, F., & Basri, G. 2003, *AJ*, 126, 1526
- Burgasser, A. J. 2007, *ApJ*, 659, 655
- Burgasser, A. J., Burrows, A., & Kirkpatrick, J. D. 2006, *ApJ*, 639, 1095
- Burgasser, A. J., Cruz, K. L., Cushing, M., Gelino, C. R.,Looper, D. L., Faherty, J. K., Kirkpatrick, J. D., & Reid, I. N. 2010, *ApJ*, 710, 1142
- Burgasser, A. J., Geballe, T. R., Leggett, S. K., Kirkpatrick, J. D., & Golimowski, D. A. 2006a, *ApJ*, 637, 1067

- Burgasser, A. J., Kirkpatrick, J. D., Cruz, K. L., Reid, I. N., Leggett, S. K., Liebert, J., Burrows, A., & Brown, M. E. 2006b, *ApJS*, 166, 585
- Burgasser, A. J., Liu, M. C., Ireland, M. J., Cruz, K. L., & Dupuy, T. J. 2008a, *ApJ*, 681, 579
- Burgasser, A. J., Looper, D. L., Kirkpatrick, J. D., Cruz, K. L., & Swift, B. J. 2008b, *ApJ*, 674, 451
- Burgasser, A. J., Looper, D. L., Kirkpatrick, J. D., & Liu, M. C. 2007, *ApJ*, 658, 557
- Burgasser, A. J., & McElwain, M. W. 2006, *AJ*, 131, 1007
- Burgasser, A. J., McElwain, M. W., Kirkpatrick, J. D., Cruz, K. L., Tinney, C. G., & Reid, I. N. 2004, *AJ*, 127, 2856
- Burningham, B., et al. 2010, *MNRAS*, 406, 1885
- Chiu, K., Fan, X., Leggett, S. K., Golimowski, D. A., Zheng, W., Geballe, T. R., Schneider, D. P., & Brinkmann, J. 2006, *AJ*, 131, 2722
- Cruz, K. L., et al. 2007, *AJ*, 133, 439
- Cushing, M. C., et al. 2008, *ApJ*, 678, 1372
- Cushing, M. C., Rayner, J. T., & Vacca, W. D. 2005, *ApJ*, 623, 1115
- Cushing, M. C., Vacca, W. D., & Rayner, J. T. 2004, *PASP*, 116, 362
- Cutri, R. M., et al. 2003, 2MASS All Sky Catalog of point sources. (The IRSA 2MASS All-Sky Point Source Catalog, NASA/IPAC Infrared Science Archive. <http://irsa.ipac.caltech.edu/applications/Gator/>)
- Delfosse, X., et al. 2004, in *Astronomical Society of the Pacific Conference Series*, Vol. 318, *Spectroscopically and Spatially Resolving the Components of the Close Binary Stars*, ed. R. W. Hilditch, H. Hensberge, & K. Pavlovski, 166
- Duquennoy, A., & Mayor, M. 1991, *A&A*, 248, 485
- Duval, V. G., Irace, W. R., Mainzer, A. K., & Wright, E. L. 2004, in *Optical, Infrared, and Millimeter Space Telescopes*. Edited by Mather, John C. *Proceedings of the SPIE*, Volume 5487, pp. 101-111 (2004)., ed. J. C. Mather, 101
- Faherty, J. K., Burgasser, A. J., Cruz, K. L., Shara, M. M., Walter, F. M., & Gelino, C. R. 2009, *AJ*, 137, 1

- Fan, X., et al. 2001, *AJ*, 122, 2833
- Fischer, D. A., & Marcy, G. W. 1992, *ApJ*, 396, 178
- Fukugita, M., Ichikawa, T., Gunn, J. E., Doi, M., Shimasaku, K., & Schneider, D. P. 1996, *AJ*, 111, 1748
- Geballe, T. R., et al. 2002, *ApJ*, 564, 466
- Gelino, C. R., Kulkarni, S. R., & Stephens, D. C. 2006, *PASP*, 118, 611
- Goldman, B., Bouy, H., Zapatero Osorio, M. R., Stumpf, M. B., Brandner, W., & Henning, T. 2008, *A&A*, 490, 763
- Hawley, S. L., et al. 2002, *AJ*, 123, 3409
- Horne, K. 1986, *PASP*, 98, 609
- Kirkpatrick, J. D., Barman, T. S., Burgasser, A. J., McGovern, M. R., McLean, I. S., Tinney, C. G., & Lowrance, P. J. 2006, *ApJ*, 639, 1120
- Kirkpatrick, J. D., Henry, T. J., & McCarthy, D. W., Jr. 1991, *ApJS*, 77, 417
- Kirkpatrick, J. D., et al. 1999, *ApJ*, 519, 802
- Kirkpatrick, J. D., et al. 2000, *AJ*, 120, 447
- Knapp, G. R., et al. 2004, *AJ*, 127, 3553
- Koerner, D. W., Kirkpatrick, J. D., McElwain, M. W., & Bonaventura, N. R. 1999, *ApJ*, 526, L25
- Kouwenhoven, M. B. N., Brown, A. G. A., Portegies Zwart, S. F., & Kaper, L. 2007, *A&A*, 474, 77
- Kouwenhoven, M. B. N., Brown, A. G. A., Zinnecker, H., Kaper, L., & Portegies Zwart, S. F. 2005, *A&A*, 430, 137
- Kroupa, P. 2002, *Science*, 295, 82
- Lawrence, A., et al. 2007, *MNRAS*, 379, 1599
- Leinert, C., Henry, T., Glindemann, A., & McCarthy, D. W., Jr. 1997, *A&A*, 325, 159
- Liu, M. C., & Leggett, S. K. 2005, *ApJ*, 634, 616

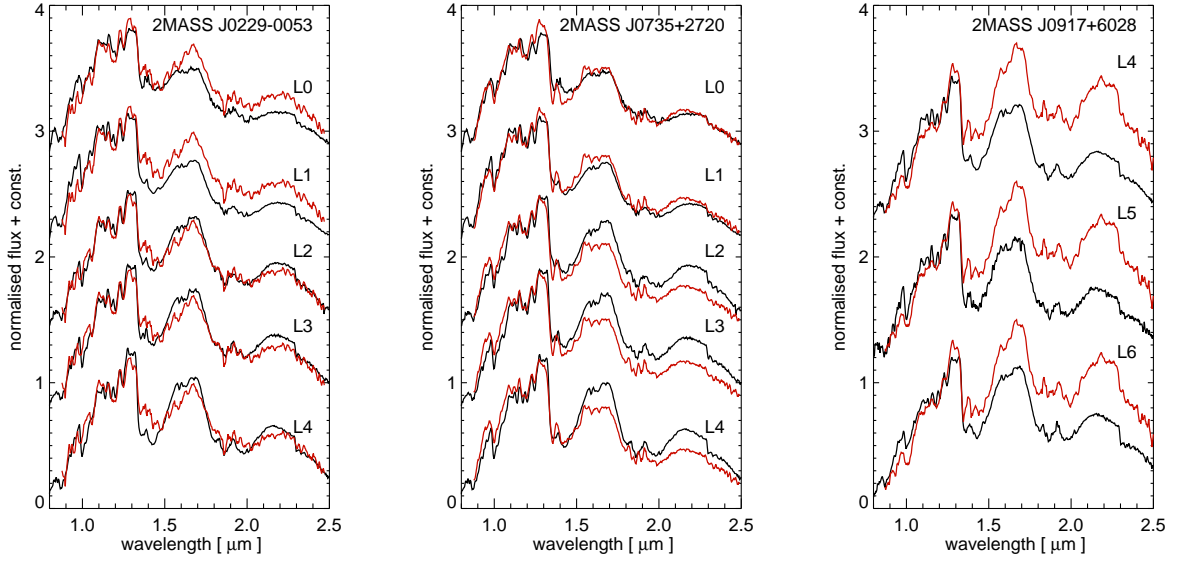
- Lodieu, N., et al. 2007, MNRAS, 379, 1423
- Looper, D. L., Gelino, C. R., Burgasser, A. J., & Kirkpatrick, J. D. 2008a, ApJ, 685, 1183
- Looper, D. L., Kirkpatrick, J. D., & Burgasser, A. J. 2007, AJ, 134, 1162
- Looper, D. L., et al. 2008b, ApJ, 686, 528
- Martin, E. L., Brandner, W., & Basri, G. 1999, Science, 283, 1718
- McLean, I. S., McGovern, M. R., Burgasser, A. J., Kirkpatrick, J. D., Prato, L., & Kim, S. S. 2003, ApJ, 596, 561
- Metchev, S. A., & Hillenbrand, L. A. 2009, ApJS, 181, 62
- Metchev, S. A., Kirkpatrick, J. D., Berriman, G. B., & Looper, D. 2008, ApJ, 676, 1281
- Mortlock, D. J., et al. 2009, A&A, 505, 97
- Pinfield, D. J., et al. 2008, MNRAS, 390, 304
- Press, W. H., Teukolsky, S. A., Vetterling, W. T., & Flannery, B. P. 1992, Numerical Recipes in Fortran 77 (New York: Cambridge Univ. Press)
- Rayner, J. T., Toomey, D. W., Onaka, P. M., Denault, A. J., Stahlberger, W. E., Vacca, W. D., Cushing, M. C., & Wang, S. 2003, PASP, 115, 362
- Rebassa-Mansergas, A., Gänsicke, B. T., & Koester, D. 2009, Journal of Physics Conference Series, 172, 012025
- Reid, I. N., Gizis, J. E., Kirkpatrick, J. D., & Koerner, D. W. 2001, AJ, 121, 489
- Reid, I. N., Lewitus, E., Burgasser, A. J., & Cruz, K. L. 2006, ApJ, 639, 1114
- Reylé, C., et al. 2010, A&A, 522, A112
- Robertson, J. G. 1986, PASP, 98, 1220
- Shatsky, N., & Tokovinin, A. 2002, A&A, 382, 92
- Sheppard, S. S., & Cushing, M. C. 2008, AJ, accepted; ArXiv:0809.0697
- Skrutskie, M. F., et al. 2006, AJ, 131, 1163
- Steele, P., Burleigh, M., Barstow, M., Jameson, R., & Dobbie, P. 2009, Journal of Physics Conference Series, 172, 012058

Stoughton, C., et al. 2002, AJ, 123, 485

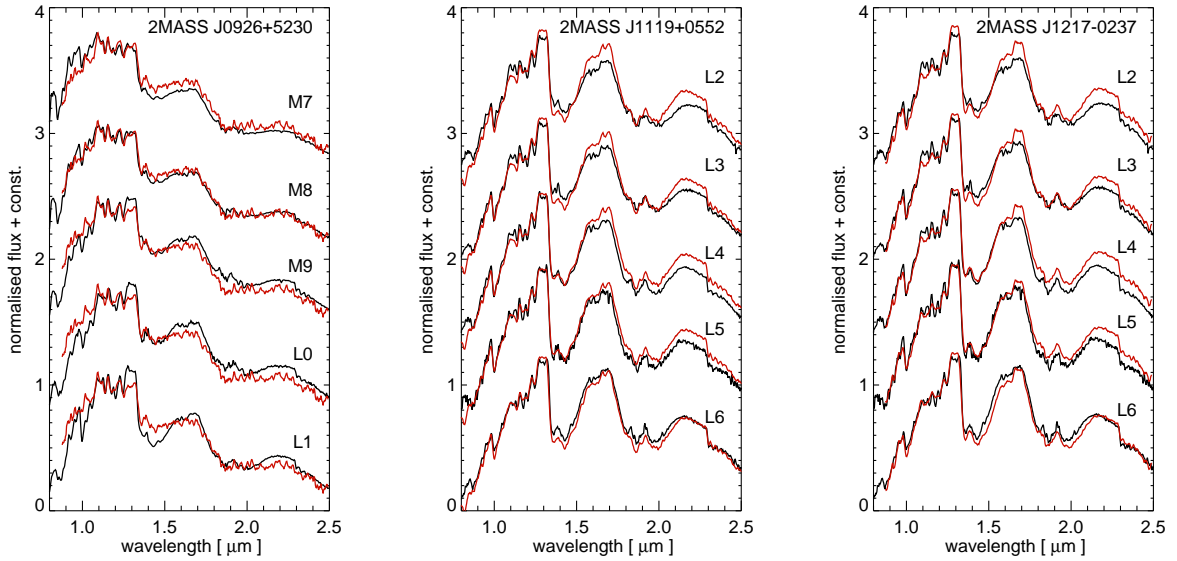
Vacca, W. D., Cushing, M. C., & Rayner, J. T. 2003, PASP, 115, 389

Zhang, Z. H., et al. 2010, MNRAS, 404, 1817

Fig. 1.— Comparison of the spectra of the discovered dwarfs (red) to the M and L dwarf standards (black). The new object spectra have been normalized to the average flux in the 1.2-1.25 μm region. In each panel the science target spectrum is reproduced multiple times with constant offsets in between. The spectra of the standards are normalized to minimum χ^2 deviations from the respective science spectrum over the 0.95-1.35 μm range.

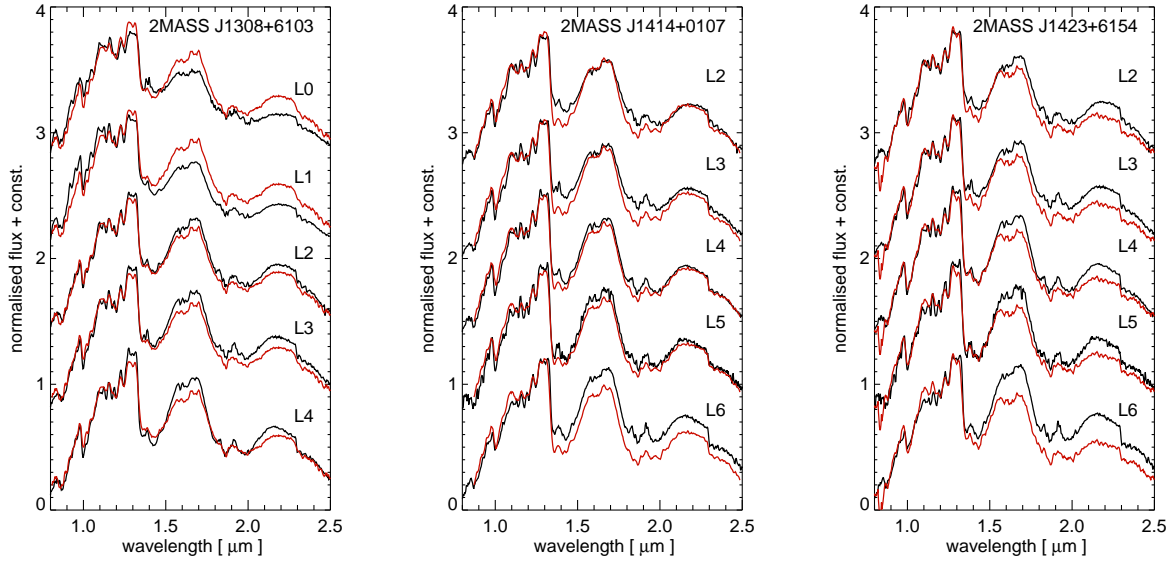


(a) 2MASS J0229–0053 (L2), 2MASS J0735+2720 (L1) and 2MASS J0917+6028 (L5).

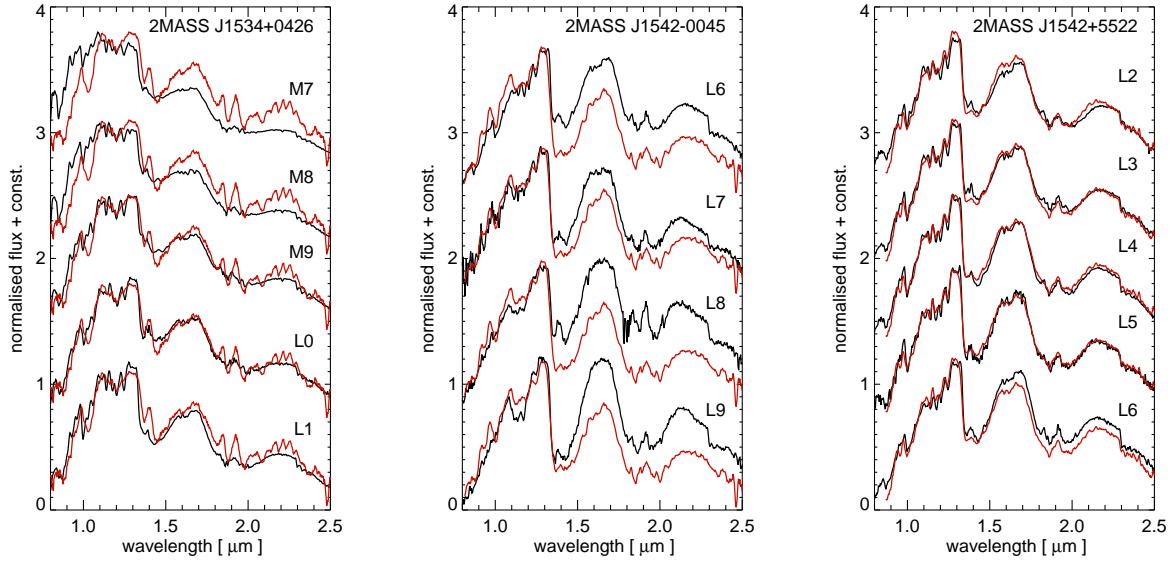


(b) 2MASS J0926+5230 (M8), 2MASS J1119+0552 (L4) and 2MASS J1217–0237 (L4).

Fig. 1.— continued.

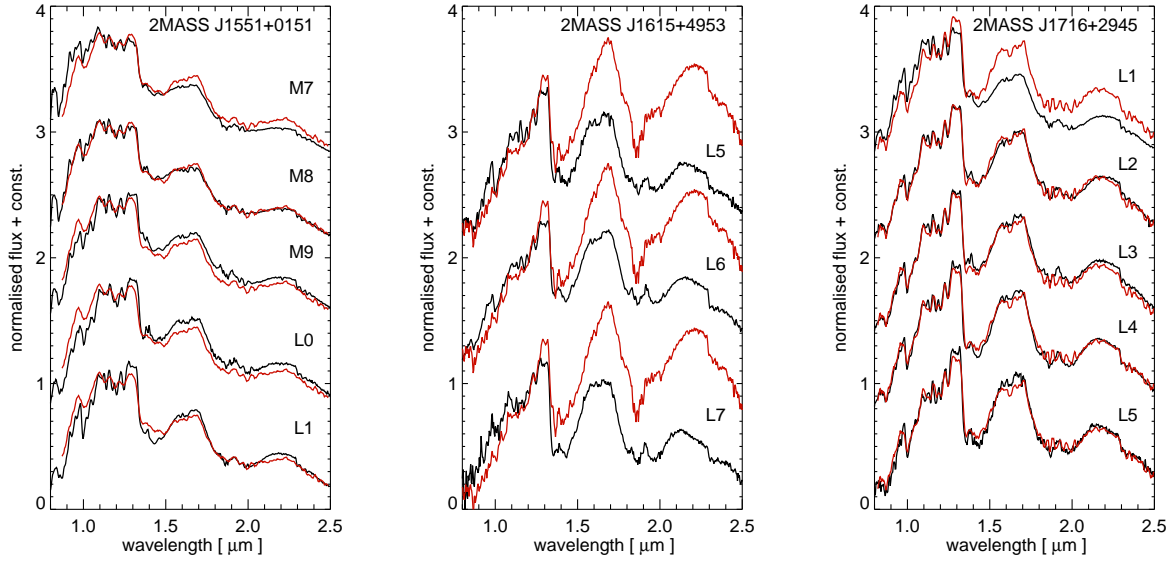


(c) 2MASS J1308+6103 (L2), 2MASS J1414+0107 (L4) and 2MASS J1423+6154 (L4).

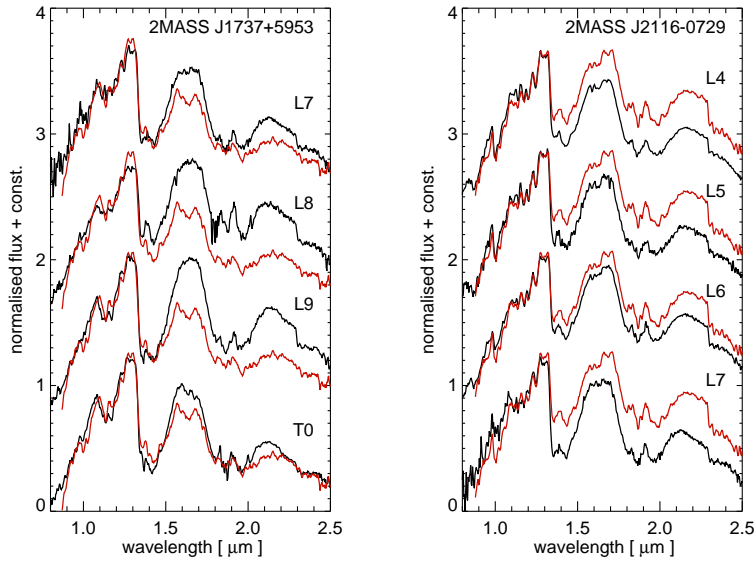


(d) 2MASS J1534+0426 (L0), 2MASS J1542-0045 (L7) and 2MASS J1542+5522 (L4).

Fig. 1.— continued.



(e) 2MASS J1551+0151 (M8), 2MASS J1615+4953 (L6) and 2MASS J1716+2945 (L3).



(f) 2MASS J1737+5953 (L9) and 2MASS J2116-0729 (L6).

Fig. 2.— Probable binary candidates from the SDSS DR1 and 2MASS PSC cross-match L dwarf sample. The first two columns compare the target spectrum (black) to best χ^2 fit single and composite templates (green) over the complete 0.95–2.35 μm range. Thereby the left column shows the best fit single template, while the middle column shows the best fit composite spectra, composed of the stated single templates (blue and red). Lastly, the right column shows the best 0.95–1.35 μm χ^2 fit. The binary candidate spectra (black) are normalized to the average flux in the 1.2–1.25 μm region, while the best-fit single and composite templates are normalized to minimum χ^2 deviations.

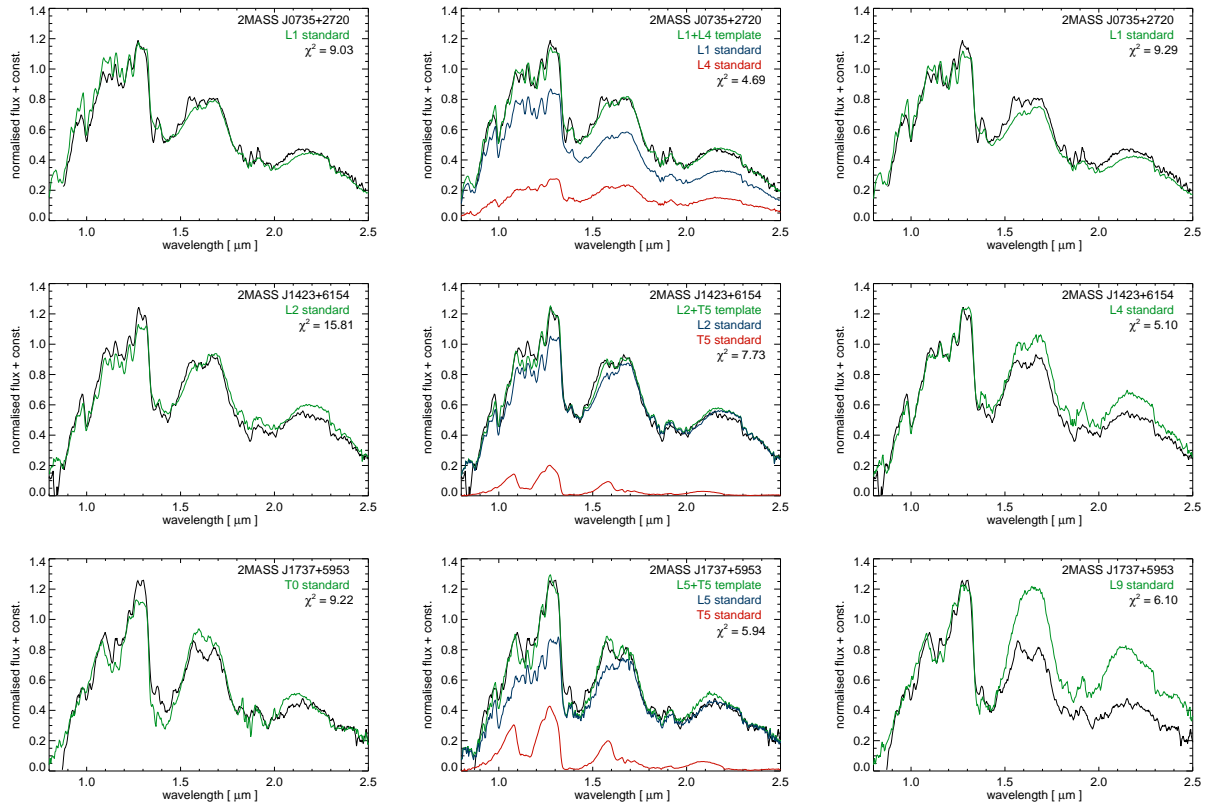


Fig. 3.— Additional binary candidates from Paper I. The left column shows the best-fit single template (green) compared to the targets spectrum (black), while the right column shows the best-fit composite template (green), along with the associated primary and secondary (blue and red, respectively). The binary candidate spectra are normalized to the average flux in the 1.2-1.25 μm region and the χ^2 fit is performed over the wavelength range of 0.95–2.35 μm . The best-fit single and composite templates are normalized to minimum χ^2 deviations.

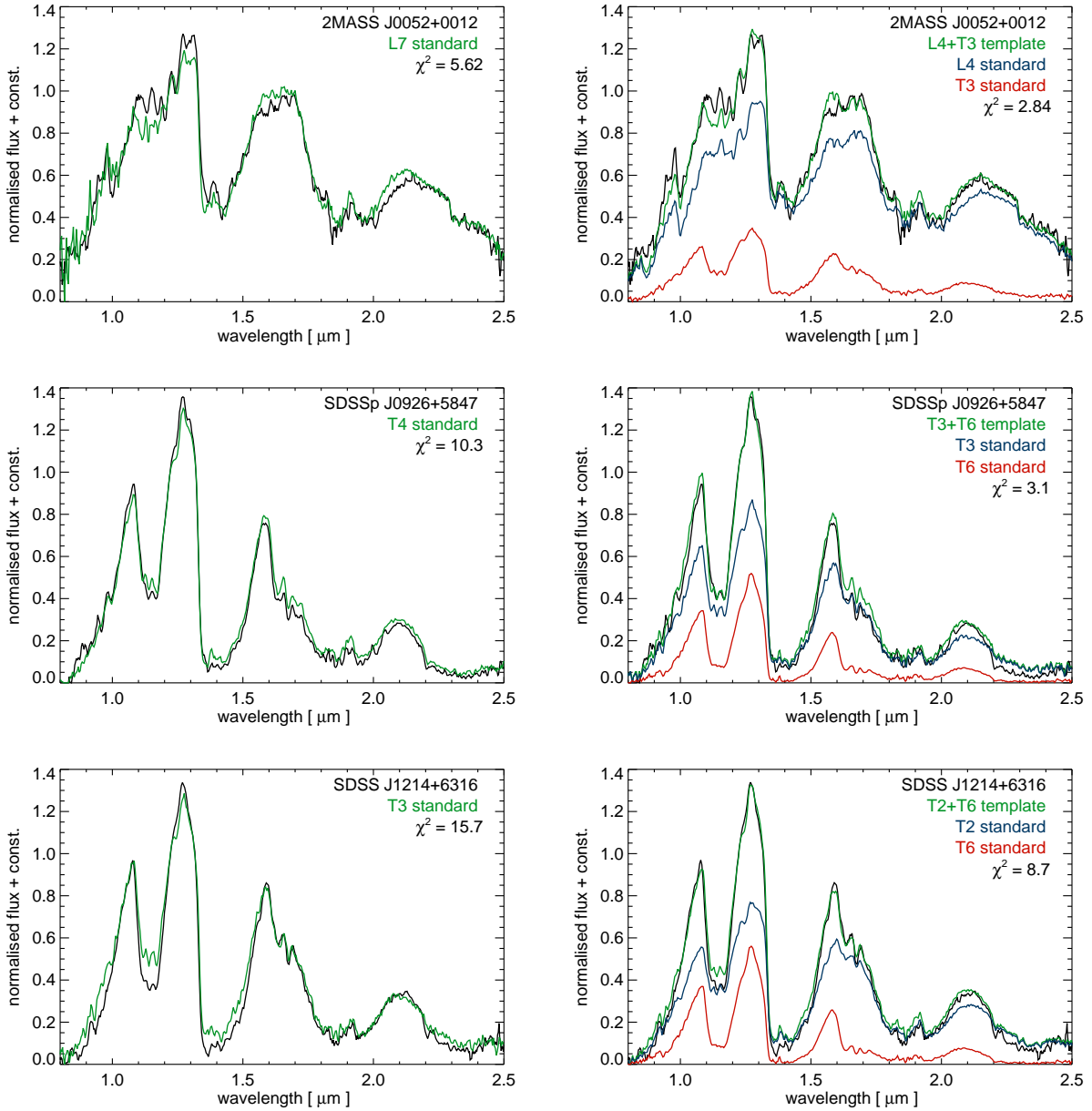


Fig. 3.— continued.

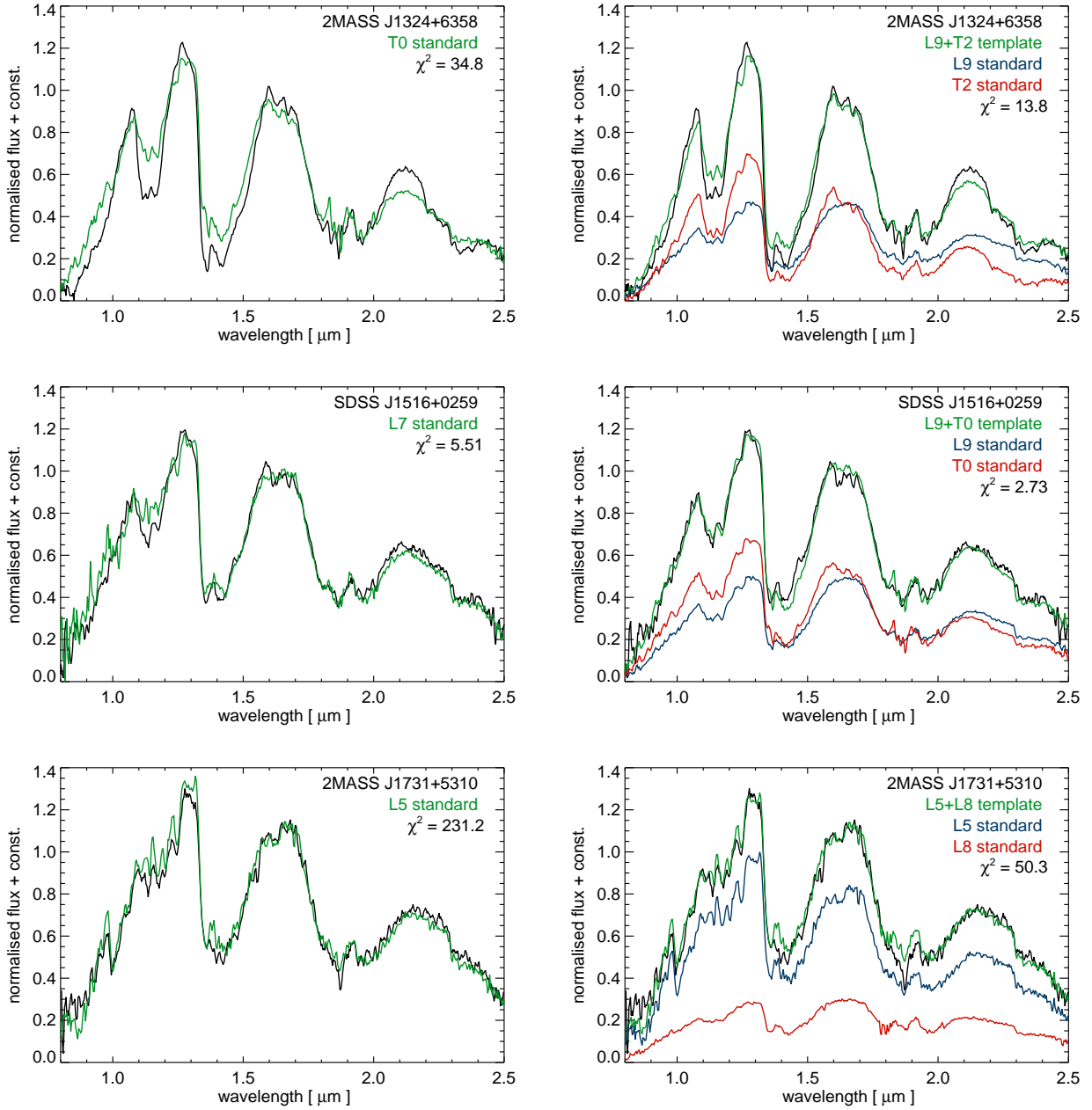


Fig. 4.— Comparison of 2MASS J1542–0045 (solid spectra) to the known blue dwarf SDSS J112118.57+433246.5 (L7.5), and to the L7 (2MASS J0205–1159) and the L8 (2MASS J1632+1904) standards from Kirkpatrick et al. (1999), which are shown as dotted lines. All spectra have been normalized to the average flux in the 1.2–1.25 μm region.

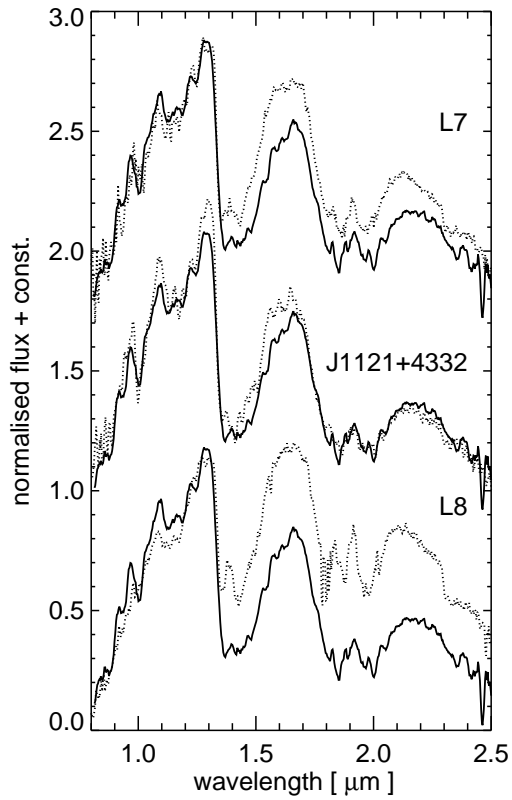


Fig. 5.— Comparison of 2MASS J0229–0053, 2MASS J0917+6028 and 2MASS J1615+4953 (red) to an ordinary L2 dwarf and to the young L2 dwarf G196–3B (dotted lines; Allers et al. 2007). All spectra have been normalized to the average flux in the 1.2–1.25 μm region.

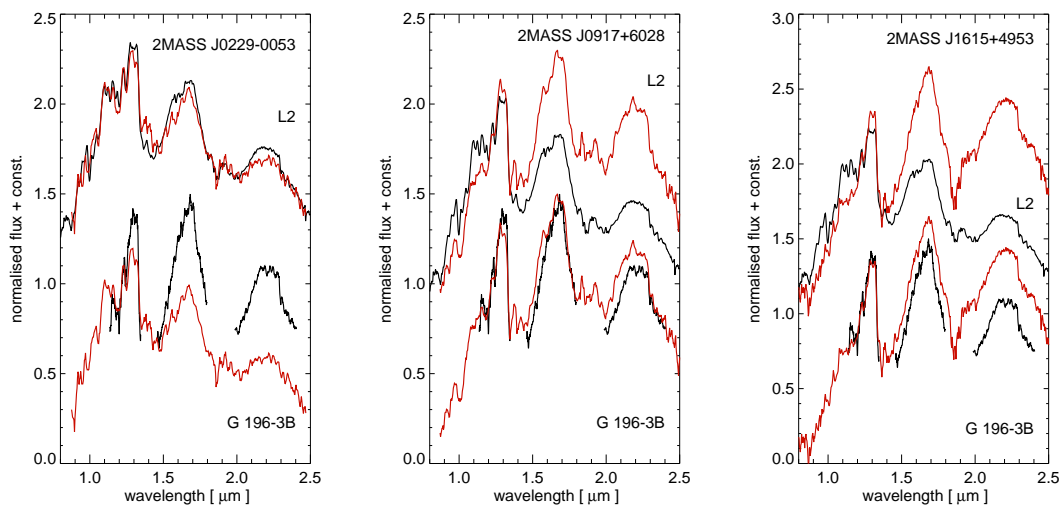


Fig. 6.— Comparison of 2MASS J0917+6028 and 2MASS J1615+4953 to the red L0 dwarf 2MASS J0141–4633 (Kirkpatrick et al. 2006). All spectra have been normalized to the average flux in the 1.15–1.3 μm region.

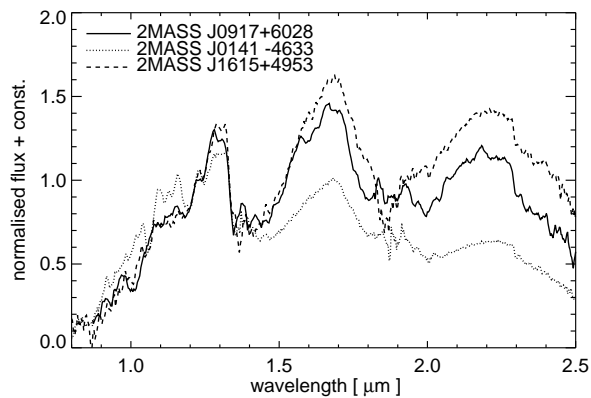


Fig. 7.— 2MASS colors vs. synthetic colors calculated from the SpeX spectra.

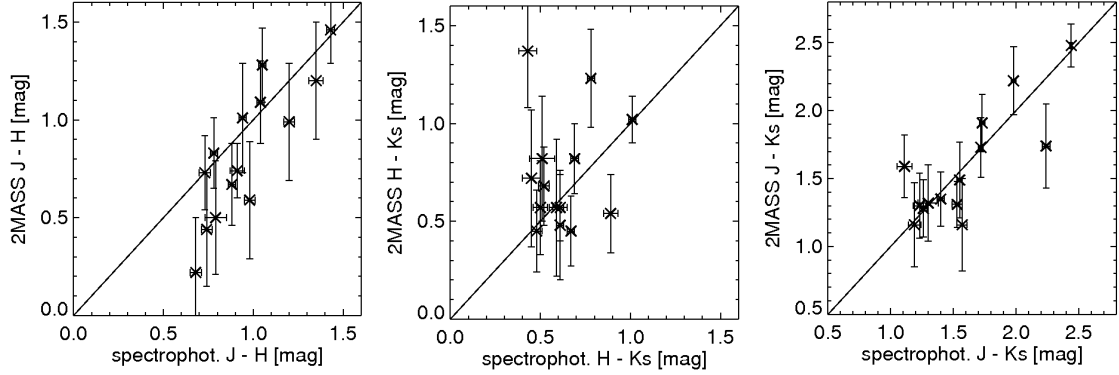


Table 1. L Dwarf Candidate Sample with SDSS and 2MASS Photometry[†].

2MASS ID (J2000)	$i - z$ [mag]	$z - J$ [mag]	$J - H$ [mag]	$H - K_S$ [mag]	$J - K_S$ [mag]	J [mag]
02292794–0053282	2.16±0.13	2.91±0.12	0.74±0.14	0.57±0.17	1.31±0.17	16.49±0.10
07354882+2720167	1.73±0.16	3.03±0.17	0.83±0.18	0.45±0.21	1.28±0.21	16.94±0.13
09175418+6028065	>2.36	3.48±0.32	1.20±0.30	0.54±0.20	1.74±0.31	17.16±0.27
09264992+5230435	1.50±0.27	2.88±0.28	< 1.19	...	< 1.57	16.77±0.14
11191046+0552484	2.11±0.13	2.88±0.17	1.28±0.19	0.45±0.18	1.73±0.22	16.76±0.16
12172372–0237369	2.20±0.21	2.99±0.19	1.09±0.21	0.82±0.18	1.91±0.21	16.90±0.16
13081228+6103486	2.00±0.14	2.75±0.19	0.51±0.26	<0.67	<1.18	16.67±0.15
14140586+0107102	2.14±0.17	2.86±0.22	1.01±0.28	0.48±0.28	1.49±0.28	16.74±0.20
14232186+6154005	2.17±1.25	2.93±0.19	0.67±0.21	0.68±0.20	1.35±0.20	16.63±0.15
15341068+0426410	1.79±0.11	2.86±0.18	0.50±0.29	0.82±0.32	1.32±0.28	16.92±0.17
15422494+5522451	1.92±0.30	<3.4	>1.18	<0.76	...	>17.13
15423630–0045452	2.41±0.15	2.75±0.14	0.73±0.19	0.57±0.24	1.30±0.24	16.71±0.13
15513546+0151129	1.78±0.15	2.77±0.18	0.22±0.28	1.37±0.29	1.59±0.23	16.85±0.15
16154255+4953211	2.34±0.16	2.90±0.16	1.46±0.17	1.02±0.12	2.48±0.16	16.79±0.14
17164260+2945536	1.91±0.16	3.00±0.22	0.59±0.30	0.57±0.35	1.16±0.34	17.06±0.20
17373467+5953434	2.42±0.39	3.38±0.21	0.44±0.29	0.72±0.35	1.16±0.31	16.88±0.16
21163374–0729200	2.11±0.21	2.89±0.25	0.99±0.30	1.23±0.25	2.22±0.25	17.20±0.21

[†]SDSS i and z magnitudes are on the AB sinh system (Fukugita et al. 1996), while 2MASS JHK_s magnitudes are on the Vega system.

Table 2. Observations of Candidate L Dwarfs with IRTF/SpeX in Prism Mode

2MASS ID (J2000)	Date (UT)	J (mag)	Slit Width (arcsec)	Exposure (min)	A0 Calibrator
02292794–0053282	2007 Nov 24	16.5	0.5	36	HD 18571
07354882+2720167	2007 Nov 24	16.9	0.8	51	HD 72982
09175418+6028065	2007 Nov 24	17.2	0.8	24	HD 88132
09264992+5230435	2007 Nov 24	16.8	0.8	27	HD 88132
... †	2008 Mar 24	16.8	0.8	24	HD 93946
11191046+0552484	2008 Mar 26	16.8	0.8	36	HD 107174
12172372–0237369	2008 Mar 25	16.9	0.8	60	HD 109969
13081228+6103486	2008 Mar 26	16.7	0.8	69	HD 120828
14140586+0107102	2008 Mar 25	16.7	0.8	60	HD 132660
14232186+6154005	2008 Mar 26	16.6	0.8	39	HD 120828
15341068+0426410	2008 Mar 27	16.9	0.8	72	HD 152115
15422494+5522451	2008 Mar 24	... ‡	0.8	60	HD 155838
15423630–0045452	2008 Mar 27	16.7	0.8	42	HD 152115
15513546+0151129	2008 Mar 25	16.9	0.8	27	HD 132660
16154255+4953211	2007 Aug 26	16.8	0.5	60	HD 160883
17164260+2945536	2007 Aug 26	17.1	0.5	48	HD 160883
17373467+5953434	2008 Mar 26	16.9	0.8	42	HD 176893
21163374–0729200	2007 Aug 26	17.2	0.5	42	HD 210781

†Repeat observation of the same object, combined with the previous data.

‡No 2MASS J detection. $H = 16.0$ mag.

Table 3. Adopted M, L, and T dwarf spectroscopic standards.

Object	Spectral Type	Ref.	$J - K_s$ (mag)	$\langle J - K_s \rangle_{\text{SpT}}^\dagger$ (mag)	$\langle z - J \rangle_{\text{SpT}}^\dagger$ (mag)	Notes
Optical spectral standards						
VB 8	M7 V	1, 2	0.96 ± 0.04	1.07 ± 0.27	1.92 ± 0.17	
VB 10	M8 V	1, 3	1.14 ± 0.03	1.10 ± 0.20	2.07 ± 0.40	
LHS 2924	M9 V	1, 4	1.25 ± 0.03	1.15 ± 0.19	2.13 ± 0.16	
2MASSP J0345432+254023	L0	5, 4	1.34 ± 0.04	1.33 ± 0.24	2.31 ± 0.14	
2MASSW J1439284+192915	L1	5, 6	1.21 ± 0.03	1.34 ± 0.24	2.46 ± 0.24	
Kelu-1	L2	5, 7	1.67 ± 0.03	1.49 ± 0.24	2.55 ± 0.18	binary ^a
2MASSW J1146345+223053	L3	5, 8	1.58 ± 0.04	1.60 ± 0.25	2.68 ± 0.24	binary ^b
2MASSI J1104012+195921	L4	3	1.43 ± 0.04	1.63 ± 0.38	2.64 ± 0.43	
DENIS-P J1228.2-1547	L5	5, 8	1.61 ± 0.04	1.73 ± 0.36	2.64 ± 0.41	binary ^c
2MASSI J1010148-040649	L6	9	1.89 ± 0.07	1.72 ± 0.29	2.63 ± 0.34	
DENIS-P J0205.4-1159	L7	5, 9	1.59 ± 0.04	1.60 ± 0.73	2.64 ± 0.23	binary ^d
2MASSW J1632291+190441	L8	5, 6	1.86 ± 0.08	1.72 ± 0.32	2.78 ± 0.41	
Near-IR spectral standards						
2MASSW J0310599+164816	L9	10, 11	1.71 ± 0.11	1.65 ± 0.29	2.75 ± 0.16	
SDSS J120747.17+024424.8	T0	10, 12	1.59 ± 0.10	1.53 ± 0.33	2.81 ± 0.42	
SDSS J015141.69+124429.6	T1	10, 3	1.38 ± 0.23	1.37 ± 0.26	2.65 ± 0.78	
SDSSp J125453.90-012247.4	T2	10, 3	1.05 ± 0.06	1.03 ± 0.48	3.02 ± 0.20	
2MASS J12095613-1004008	T3	10, 3	0.85 ± 0.16	0.97 ± 0.39	2.99 ± 0.13	
2MASSI J2254188+312349	T4	10, 3	0.36 ± 0.15	0.60 ± 0.23	3.25 ± 0.27	
2MASS J15031961+2525196	T5	10, 3	-0.03 ± 0.06	0.22 ± 0.43	3.34 ± 0.18	
SDSSp J162414.37+002915.6	T6	10, 13	< -0.02	0.14 ± 0.38	3.43 ± 0.11	
2MASSI J0727182+171001	T7	10, 13	0.04 ± 0.20	0.05 ± 0.44	3.36 ± 0.15	
2MASSI J0415195-093506	T8	10, 3	0.27 ± 0.21	-0.1 ± 0.51	...	

[†]Mean $J - K_s$ and $z - J$ colors and their standard deviations for all objects of a given spectral type, as compiled from DwarfArchives.org (L and T dwarfs) or from the Ultracool Dwarf Catalog (M dwarfs; http://www.iac.es/galeria/ege/catalogo_espectral/).

^aLiu & Leggett (2005); Gelino et al. (2006).

^bReid et al. (2001).

^cMartin et al. (1999); Bouy et al. (2003).

^dKoerner et al. (1999); Bouy et al. (2003).

References. — 1–Kirkpatrick et al. (1999), 2–Burgasser et al. (2008a), 3–Burgasser et al. (2004), 4–

Burgasser & McElwain (2006), 5–Kirkpatrick et al. (1999), 6–Burgasser et al. (2004), 7–Burgasser et al. (2007), 8–Burgasser et al. (2010), 9–Reid et al. (2006), 10–Burgasser et al. (2006a), 11–Burgasser (2007), 12–Looper et al. (2007), 13–Burgasser et al. (2006).

Table 4. Spectral classification of single and candidate binary L and T dwarfs, including candidate binaries from Paper I.

Object	0.95–1.35 μm χ^2 fit (adopted if single)	0.95–2.35 μm χ^2 fit (adopted if binary)	Note
New L Dwarfs			
2MASS J02292794–0053282	L2	L2	
2MASS J07354882+2720167	L1	L1+L4	binary
2MASS J09175418+6028065	L5	L8	red
2MASS J09264992+5230435	M8	M8	
2MASS J11191046+0552484	L4	L6	
2MASS J12172372–0237369	L4	L6	
2MASS J13081228+6103486	L2	L2	
2MASS J14140586+0107102	L4	L4	
2MASS J14232186+6154005	L4	L2+T5	binary
2MASS J15341068+0426410	L0	L0	
2MASS J15423630–0045452	L7	L1	blue
2MASS J15422494+5522451	L4	L4	
2MASS J15513546+0151129	M8	M8	
2MASS J16154255+4953211	L6	L8	red/young
2MASS J17164260+2945536	L3	L3	
2MASS J17373467+5953434	L9	L5+T5	blue/binary
2MASS J21163374–0729200	L6	L8	
Peculiar Dwarfs or Binary Candidates from Paper I[†]			
2MASS J00521232+0012172	L5 [*]	L4+T3	binary
SDSSp J010752.33+004156.1	L8	L8	red
2MASS J01262109+1428057	L6 [‡]	L8	red/young
SDSS J092615.38+584720.9	T4	T3+T6	binary
SDSS J121440.95+631643.4	T5	T2+T6	binary
2MASS J13243559+6358284	T3	L9+T2	red/binary
SDSS J151603.03+025928.9	T0	L9+T0	binary
2MASS J17310140+5310476	L5	L5+L8	binary

Note. — The spectral types are determined from minimum χ^2 fitting over the 0.95–1.35 μm and the 0.95–2.35 μm regions. The former fit yields the adopted spectral type for each individual object, listed in the second column. The latter fit yields the adopted spectral type combination for candidate unresolved binary systems.

[†]Our 0.95–1.35 μm spectral classifications for the previously identified L and T dwarfs

differ from the ones published or referenced in Paper I by ≤ 2 subtypes, unless noted.

*Classified as an L2 dwarf in Paper I by comparison of the 0.8–1.3 μm region to L dwarf standards from Cushing et al. (2005)

‡Classified as an L2 dwarf in Paper I by direct comparison to the peculiarly red L2 dwarf G 196–3B.

Table 5. List of best-fit composite spectral types for probable binary candidates.

Object	Primary	Secondary	fraction [†] [%]
New Binaries Presented Here			
2MASS J07354882+2720167	L1	L4	75.4
	L1	L5	22.0
2MASS J14232186+6154005	L2	T5	55.6
	L2	T4	41.6
2MASS J17373467+5953434	L5	T5	79.4
	L4	T5	19.2
Binaries from Paper I			
2MASS J00521232+0012172	L4	T3	53.0
	L2	T3	43.3
SDSS J092615.38+584720.9	T3	T6	54.0
	T4	T6	46.0
SDSS J121440.95+631643.4	T2	T6	78.9
	T3	T8	21.1
2MASS J13243559+6358284	L9	T2	99.3
SDSS J151603.03+025928.9	L9	T0	53.4
	L8	T0	46.6
2MASS J17310140+5310476	L5	L8	100.

[†]The last column gives the percentage of cases the composite template has been returned as the best-fit combination during Monte Carlo simulations (§ 3.2).